Nonlinear charge transport mechanism in periodic and disordered DNA

D. Hennig [b,1], J.F.R. Archilla [a], J. Agarwal [b],

[a] *Departamento de Física Aplicada I. Universidad de Sevilla. Avda. Reina Mercedes, s/n. 41012-Sevilla, Spain*

[b] *Freie Universität Berlin, Fachbereich Physik, Institut für Theoretische Physik. Arnimallee 14, 14195 Berlin, Germany*

Abstract

We study a model for polaron-like charge transport mechanism along DNA molecules with emphasis on the impact of parametrical and structural disorder. Our model Hamiltonian takes into account the coupling of the charge carrier to two different kind of modes representing fluctuating twist motions of the base pairs and H-bond distortions within the double helix structure of $\lambda-$DNA. Localized stationary states are constructed with the help of a nonlinear map approach for a periodic double helix and in the presence of intrinsic static parametrical and/or structural disorder reflecting the impact of ambient solvent coordinates. It is demonstrated that charge transport is mediated by moving polarons respectively breather compounds carrying not only the charge but causing also local temporal deformations of the helix structure through the traveling torsion and bond breather components illustrating the interplay of structure and function in biomolecules.

Key words:
PACS: 87.-15.v,, 63.20.Kr, 63.20.Ry

1 Introduction

Electronic transport through DNA is crucial for its biological functions such as the repair mechanism after radiation damage and biosynthesis. As proposed in [1] electron transport through DNA proceeds along a one-dimensional pathway constituted by the overlap between $\pi-$orbitals in neighboring base pairs.

[1] Corresponding author. E-mail:hennigd@physik.fu-berlin.de

With the perspective to possible applications in molecular electronics biomaterials are supposed to play an important role because they may offer the ultimate way to miniaturization and their attributed electrical transport properties are expected to be markedly different from those of traditional macroscopic conductors [2]. In this context enormous effort has been directed towards investigations of conductivity of DNA viewed as a promising conduit for charge transport on nanoscales [3]. So far the findings concerning conductivity of DNA have been controversial. There are the results of recent measurements indicating that DNA behaves as a well conducting one-dimensional molecular wire [4]-[10]. In contrast it was reported that DNA is insulating [11] and for short oligomers built up from base pairs of the same type semiconductivity was observed [12]. This qualitative discrepancy is shared also by theoretical findings so that it remains unclear whether DNA is conductive or not. For example a theoretical investigation based on first principle calculations suggests the absence of dc-conductivity in DNA [13]. On the other hand there stand the studies using various assumptions for modeling the DNA structure which focus on different aspects such as the influence of aperiodicity, temperature driven fluctuations and aggregation effects on the energetic control of charge migration which have all come to the conclusion that DNA is a conductor [14]-[18].

The detailed understanding of the conduction mechanism of DNA remains still an unsolved task. Different attempts to model the charge transport of DNA were based on transport via coherent tunneling [1], classical diffusion under the conditions of temperature-driven fluctuations [16], incoherent phonon-assisted hopping [19],[20], variable range hopping between localized states [17] and charge carriages mediated by polarons [21],[22] and solitons [23].

In the present work we use for the theoretical description of charge transport in DNA a nonlinear approach facilitating the concept of polaron respectively breather solutions. The structure of the bent double helix of $\lambda-$DNA is modeled by a sterical network of oscillators in the frame of the base pair picture [24],[25],[26] taking into account deformations of the hydrogen bonds within a base pair and twist motions between adjacent base pairs. The electron motion is described by a tight-binding system. It is assumed that the electron motion is predominantly influenced by vibrational modes of the double helix. The nonlinear interaction between the electron and the vibrational modes causes the formation of polarons respectively electron-vibron breathers supporting charge localization and transport.

The aim of the current investigation is to elucidate the role played by static parametrical disorder and complex structural effects due to irregular deviations from the ordered helical shape of the double helix (reflected in random arrangements of the positions of the bases) with regard to the charge transport in DNA. There arises at least one interesting question, namely: Is

long-lived and stable charge transport in DNA achievable at all under the impact of disorder ? To tackle this problem in our paper we exploit analytical and numerical methods from the theory of (nonlinear) dynamical systems in combination with the theory of (linear) disordered systems. The paper is organized as follows: In the first section we describe the model for the charge transport along the steric structure of the bent DNA double helix. The second section is concerned with the construction of polaron respectively static electron-vibron breather solutions of the nonlinear lattice system when parametrical and structural disorder effects are taken into account. In section 4 we discuss the mobility properties of the polarons respectively electron-vibron breathers and their transport efficiency in dependence on the degree of disorder contained in the on-site energies and/or in structural arrangements of the helix. In a subsequent section

we invoke the Floquet analysis to explain also the mobility of the polarons and breathers in terms of their spectral properties. Finally, we present a summary and discussion of the results.

2 Model Hamiltonian for charge transfer along DNA

DNA chains are quite flexible and exhibit structural fluctuations influencing the transport properties. Our model is designed to cover the basic features of the DNA double helix structure needed for a proper description of the charge transport dynamics under the impact of fluctuating base motions. Despite the fact that the charge transport proceeds across a one-dimensional channel of base stacks spanning along the sugar-phosphate backbone so that DNA can effectively be viewed as a one-dimensional molecular wire [27] some significant details of the three-dimensional DNA structure have to be incorporated in the model. For the physical description of DNA molecules their detailed chemical structure can be neglected. They can be simply considered as bent double-stranded systems with an adequate number of parameters sufficient for modeling the considered physical process. In the frame of simple DNA models such as the base pair picture the bases have been treated as single nondeformable entities. The helicoidal structure of DNA is then conveniently described in a cylindrical reference system where each base pair possesses two degrees of freedom, namely a radial variable measuring the transversal displacements of the base pair (that is deformations of the H-bond) and its angle with a reference axis in a plane perpendicular to the helix backbone which defines the twist of the helix [26]. In Fig. 1 we depict schematically the structure of the DNA model.

With relevance to charge migration the most influential fluctuating motions of DNA originate from tranverse vibrations of the bases relative to each other

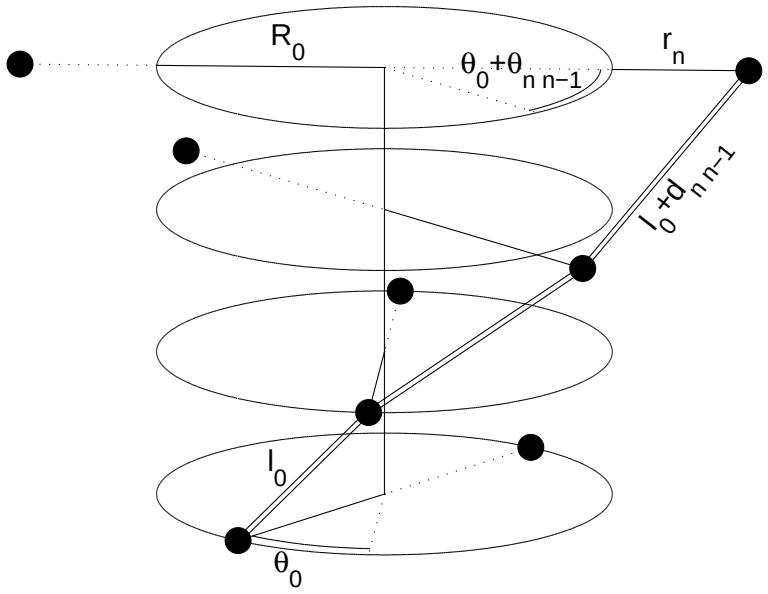

Fig. 1. Sketch of the helicoidal structure of the DNA model, the bases being represented by bullets. Geometrical parameters R_0, θ_0, l_0 and the radial and angular variables r_n and $\theta_{n\,n-1}$, respectively are indicated.

within each base plane, i.e. the base pair distance stretchings/compressions and the torsional variations of the helicoidal twist dominating longitudinal (acoustic strand) phonons [16] because the sugar-phosphate chains are rather stretch proof [27]. Therefore it is justified to discard the impact of longitudinal vibrations and the considered motion is restricted to the base pair planes [15]. Furthermore, the angular twist and radial vibrational motions evolve independently on two different time scales and can be regarded as decoupled degrees of freedom in the harmonic treatment of the normal mode vibrations of DNA [28].

The Hamiltonian for the electron migration along a strand in DNA consists of three parts

$$H = H_{el} + H_{rad} + H_{twist}\,, \tag{1}$$

with H_{el} representing the part corresponding to the particle charge transport over the base pairs, H_{rad} describes the dynamics of the H-bond vibrations and H_{twist} models the dynamics of the relative twist angle between two consecutive base pairs. The electronic part is given by a tight-binding system

$$H_{el} = \sum_n E_n \left|c_n\right|^2 - V_{n\,n-1} \left(c_n^* c_{n-1} + c_n c_{n-1}^* \right) . \tag{2}$$

The index n denotes the site of the $n-$th base on one of the two strands and c_n determines the probability that the electron occupies this site. E_n is the local electronic energy and V_{nn-1} stands for the transfer matrix element which is responsible for the transport of the electron along the stacked base pairs.

The vibronic part H_{rad} takes into account radial displacements of the base units from their equilibrium positions within the base pair plane connected with deformations of the hydrogen bonds linking two bases. The corresponding part of the Hamiltonian treating the bond vibrations classically and harmonically is given by

$$H_{rad} = \sum_n \left[\frac{(p_n^r)^2}{2\,M_n} + \frac{M_n\,\Omega_r^2\,r_n^2}{2} \right] . \tag{3}$$

with the momenta $(p_n^r)^2$ conjugate to the radial coordinates r_n measuring the deviation from the equilibrium length of a hydrogen bond along the line bridging two bases of a base pair, Ω_r is the frequency and M_n is the reduced mass of a base pair.

The twist motion part reads as

$$H_{twist} = \sum_n [\, \frac{\left(p^{\theta}_{n\,n-1}\right)^2}{2\,J_n} + \frac{J_n\,\Omega_\theta^2\,\theta^2_{n\,n-1}}{2} \,] \,, \tag{4}$$

where $\theta_{n\,n-1}$ is the relative angle between two adjacent base pairs quantifying displacements from its equilibrium twist angle θ_0 and J_n is the reduced moment of inertia.

We emphasize that in the context of charge transport in DNA the nonlinear dynamics of large amplitude structural transitions are not of interest because charge transport processes are thought to be mainly facilitated by soft fluctuational vibrational modes allowing the harmonic approximation of their dynamics.

The interaction between the electronic variable and the structure variables r_n and $\theta_{n\,n-1}$ stems from the parameter dependence of the electronic parameters E_n and $V_{n\,n-1}$. The diagonal term expressing the most efficient coupling is of the form

$$E_n = E_n^0 + k\,r_n \,, \tag{5}$$

and takes into account the modulation of the on-site electronic energy E_n^0 by the radial vibrations of the base pairs. In turn the actual charge occupation has its impact on the local radial distortion of the helix. As the transfer matrix elements $V_{n\,n-1}$ are concerned we assume that they depend on the three-dimensional distance between two consecutive bases along a strand in the following fashion

$$V_{n\,n-1} = V_0\,(1 - \alpha\,d_{n\,n-1}) \,. \tag{6}$$

The quantity α regulates how strong $V_{n\,n-1}$ is influenced by the distance and the latter is determined by

$$d_{n\,n-1} = \Big\{ a^2 + (R_0 + r_n)^2 + (R_0 + r_{n-1})^2 \\ - 2(R_0 + r_n)(R_0 + r_{n-1})\, \cos(\theta_0 + \theta_{n\,n-1}) \Big\}^{1/2} - l_0\,, \tag{7}$$

with

$$l_0 = \sqrt{a^2 + 4R_0^2\, \sin^2(\theta_0/2)}\,. \tag{8}$$

Expanding the expression (7) up to first order around the equilibrium positions gives

$$d_{n\,n-1} \simeq \frac{R_0}{l_0}\, \left[\, (\,1 - \cos\theta_0\,)\,(r_n + r_{n-1}) \,+\, \sin\theta_0\, R_0\, \theta_{n\,n-1}\,\right]\,. \tag{9}$$

Realistic parameters for DNA molecules are given by [26],[27]: $a = 3.4\mathring{A}$, $R_0 \approx 10\mathring{A}$, $\theta_0 = 36^\circ$, $J = 4.982 \times 10^{-45}\, kg\, m^2$, $\Omega_\theta = [0.526 - 0.744] \times 10^{12}\, s^{-1}$, $\Omega_r = 6.252\, \times 10^{12}\, s^{-1}$, $V_0 \simeq 0.1\, eV$ and $M = 4.982 \times 10^{-25} kg$.

We scale the time according to $t \,\rightarrow\, \Omega_r\, t$ and introduce the dimensionless quantities:

$$\tilde{r}_n = \sqrt{\frac{M\Omega_r^2}{V_0}}\, r_n\,, \qquad \tilde{k}_n = \frac{k_n}{\sqrt{M\Omega_r^2 V_0}}\,, \qquad \tilde{E}_n^0 = \frac{E_n^0}{V_0} \tag{10}$$

$$\tilde{\Omega} = \frac{\Omega_\theta}{\Omega_r}\,, \quad \tilde{V} = \frac{V_0}{J\,\Omega_r^2}\,, \quad \tilde{\alpha} = \sqrt{\frac{V_0}{M\,\Omega_r^2}}\,\alpha\,, \quad \tilde{R}_0 = \sqrt{\frac{M\,\Omega_r^2}{V_0}}\, R_0\,. \tag{11}$$

Subsequently we omit the tildes.

With the use of the expression (9) the equations of motion derived from the Hamiltonian (2)-(4) read as

$$i\,\tau \dot{c}_n = (E_n^0 \,+ k\, r_n)\, c_n \\ - (1 - \alpha\, d_{n+1,n})\, c_{n+1} - (1 - \alpha\, d_{n\,n-1})\, c_{n-1} \tag{12}$$

$$\ddot{r}_n = -r_n - k\,|c_n|^2 \,-\, \alpha\, \frac{R_0}{l_0}\,(1 - \cos\theta_0) \\ \times \Big\{\, [c_{n+1}^* c_n + c_{n+1} c_n^*] + [c_n^* c_{n-1} + c_n c_{n-1}^*] \,\Big\} \tag{13}$$

$$\ddot{\theta}_{n\,n-1} = -\Omega^2\, \theta_{n\,n-1} \,-\, \alpha\, V\, \frac{R_0^2}{l_0}\, \sin\theta_0\, [c_n^*\, c_{n-1} \,+\, c_n\, c_{n-1}^*]\,, \tag{14}$$

and the quantity $\tau = \hbar\, \Omega_r / V_0$ appearing in Eq. (12) determines the time scale separation between the fast electron motion and the slow bond vibrations. We remark that in the limit case of $\alpha = 0$ and constant $E_n^0 = E_0$ the set of coupled equations represents the Holstein system widely used in studies of polaron dynamics in one-dimensional lattices [29]. Furthermore in the linear

limit case emerging for $\alpha = k = 0$ the Anderson model is obtained for random E_n^0 [30],[31].

Regarding the dynamical energy exchange between the various degrees of freedom we state that due to the large differences between the electronic and vibronic frequencies we are able to prove rigorously that the energy exchange is suppressed on time scales growing exponentially with the ratio of the frequencies. Corresponding bounds on the energy exchange suppression are derived with the help of Nekhoroshev-like arguments [32],[33]. Furthermore applying the concept of the anti-integrable limit [34] we are able to prove the existence of breather solutions for the coupled system (12)-(14). The mathematical details are delegated to a forthcoming article [35].

The values of the scaled parameters are given by $\tau = 0.2589$, $\Omega^2 = [\,0.709 - 1.417\,] \times 10^{-2}$, $V = 0.0823$, $R_0 = 34.862$ and $l_0 = 24.590$. In our model study we treat the electron-mode coupling strengths k and α for which no reliable data are available as adjustable parameters. In the forthcoming investigations we adopt the values of these free parameters such that not too strong deformations of the helix result which is essential for our used harmonic treatment of the dynamics of the structural coordinates.

3 Localized polaron-like states

Being interested in the simulation of a nonlinear charge transport mechanism in DNA we embark as a first step on the construction of localized stationary solutions of the coupled system (12)-(14). Exploiting the fact that the adiabaticity parameter τ is small, i.e. the fast charge transport along the base stacks and the slow bond vibrations and the even slower rotational twist motions evolve on distinct time scales, the inertia in Eqs. (13) and (14) are negligible. Therefore, one can solve in the adiabatic limit the resulting static equations which results in the instantaneous displacements

$$\begin{aligned} r_n = & -k\,|c_n|^2 \;-\; \alpha\,\frac{R_0}{l_0}\,(1-\cos\theta_0) \\ & \times \Big\{\,[c_{n+1}^* c_n + c_{n+1} c_n^*] + [c_n^* c_{n-1} + c_n c_{n-1}^*]\,\Big\}\,, \end{aligned} \tag{15}$$

$$\theta_{n\,n-1} = -\frac{\alpha\,V}{\Omega^2}\,\frac{R_0^2}{l_0}\,\sin\theta_0\,[c_n^* c_{n-1} + c_n c_{n-1}^*]\,. \tag{16}$$

Upon insertion of (15) and (16) into Eq. (12) one obtains a nonlinear discrete Schrödinger equation for the electronic amplitude

$$
\begin{aligned}
i\,\tau\,\dot{c}_n = & \Big[E_n^0 - k^2\,|c_n|^2 - k\,\alpha\,\frac{R_0}{l_0}\,(1-\cos\theta_0) \\
& \times \Big\{ [c_{n+1}^* c_n + c_{n+1} c_n^*] + [c_n^* c_{n-1} + c_n c_{n-1}^*] \Big\} \Big]\; c_n \\
& - (\,1 + b_{n+1\,n}\,)\,c_{n+1} \;-\; (\,1 + b_{n\,n-1}\,)\,c_{n-1}\,, \qquad (17)
\end{aligned}
$$

with

$$
\begin{aligned}
b_{n\,n-1} = & \alpha\,\left(\frac{R_0}{l_0}\right)^2 \Big\{ (1-\cos\theta_0)\,\Big[k\,\frac{l_0}{R_0}\,[|c_n|^2 + |c_{n-1}|^2] \\
& + \alpha\,(1-\cos\theta_0)\,\Big([c_{n+1}^* c_n + c_{n+1} c_n^*] \\
& + 2\,[c_n^* c_{n-1} + c_n c_{n-1}^*] + [c_{n-1}^* c_{n-2} + c_{n-1} c_{n-2}^*] \Big) \Big] \\
& + \frac{\alpha\,V}{\Omega^2}\,R_0^2\,\sin^2\theta_0\,[c_n^* c_{n-1} + c_n c_n c_{n-1}^*] \Big\} \qquad (18)
\end{aligned}
$$

In order to search for stationary localized solutions (polaron states) we substitute $c_n = \Phi_n\,\exp[-i\,Et/\tau]$ in Eq. (17) and obtain the difference system

$$
\begin{aligned}
E\,\Phi_n = & \Big[E_n^0 - k^2\,|\Phi_n|^2 - k\,\alpha\,\frac{R_0}{l_0}\,(1-\cos\theta_0) \\
& \times \Big\{ [\Phi_{n+1}^* \Phi_n + \Phi_{n+1} \Phi_n^*] + [\Phi_n^* \Phi_{n-1} + \Phi_n \Phi_{n-1}^*] \Big\} \Big]\; \Phi_n \\
& - (\,1 + B_{n+1\,n}\,)\,\Phi_{n+1} \;-\; (\,1 + B_{n\,n-1}\,)\,\Phi_{n-1}\,, \qquad (19)
\end{aligned}
$$

where $B_{n\,n-1}$ is given by

$$
\begin{aligned}
B_{n\,n-1} = & \alpha\,\left(\frac{R_0}{l_0}\right)^2 \Big\{ (1-\cos\theta_0)\,\Big[k\,\frac{l_0}{R_0}\,[|\Phi_n|^2 + |\Phi_{n-1}|^2] \\
& + \alpha\,(1-\cos\theta_0)\,\Big([\Phi_{n+1}^* \Phi_n + \Phi_{n+1} \Phi_n^*] \\
& + 2\,[\Phi_n^* \Phi_{n-1} + \Phi_n \Phi_{n-1}^*] + [\Phi_{n-1}^* \Phi_{n-2} + \Phi_{n-1} \Phi_{n-2}^*] \Big) \Big] \\
& + \frac{\alpha\,V}{\Omega^2}\,R_0^2\,\sin^2\theta_0\,[\Phi_n^* \Phi_{n-1} + \Phi_n \Phi_{n-1}^*] \Big\} \qquad (20)
\end{aligned}
$$

The ground state of the system (19) is computed with the numerical map method outlined in [36],[37].

In Fig. 2 we depict typical patterns of polaron states. First we discuss the ordered (periodic) case arising e.g. for synthetically produced DNA molecules consisting of a single type of base pairs (e.g. poly(G)-poly(C) DNA polymers) surrounded by vacuum which provides realistic ideal conditions for the consideration of DNA conductivity in experimental and theoretical studies [12]. The

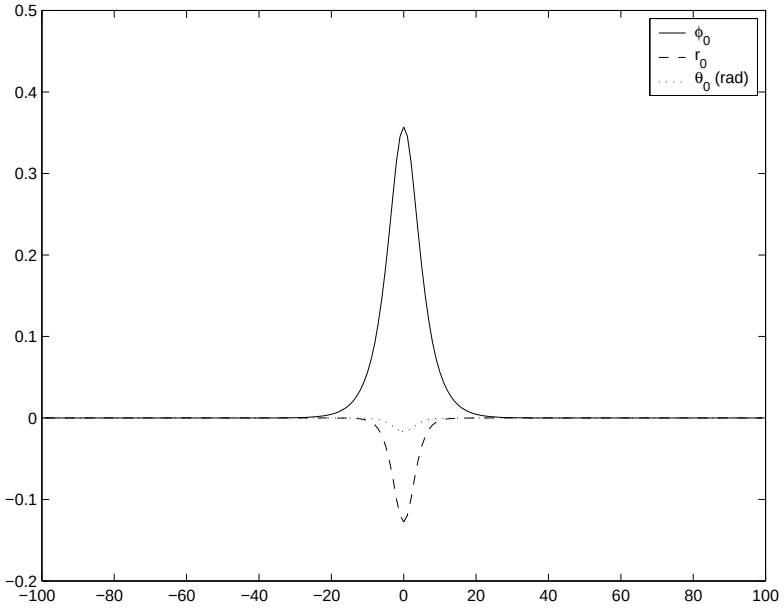

Fig. 2. Profiles of the stationary polaron states for the ordered (periodic) case.
(a) The electronic amplitudes $|\Phi_n|^2$.
(b) The static radial displacements r_n.
(c) The static angular twists θ_n.

electronic contribution is shown in Fig. 2 (a). In the ordered case the electronic wave function is localized at the central lattice site and the amplitudes decay monotonically and exponentially with growing distance from this central site. We remark that the spatial extension of the polaron decreases with increased coupling strength k and there is a smooth transition from large to small polarons. Analogously, enlarging the off-diagonal coupling strength α leads also to enhanced degree of localization. The size of the polarons plays a crucial role for their mobility in the sense that for large up to medium polarons coherent motion can be activated whereas small polarons are immobile due to their pinning to the discrete lattice [38],[39]. The associated patterns of the static radial and angular displacements of the bases are shown in Fig. 2 (b) and (c), respectively. Like the electronic wave function the radial and angular displacements are exponentially localized at the central lattice site (base pair). Notice that due to the overall minus sign of the radial and angular excitation patterns the H-bridges get compressed while the helix experiences a local unwinding around the occupation peak of the localized electron.

For a more realistic study we take static diagonal disorder in the on-site electronic energy E_n^0 into account. The random values caused for example by the inhomogeneous broadening of the sites of distinct ion pairs with different energies were simulated by random potentials $[-\Delta E, \Delta E]$ with mean value $\bar{E} = 0$ and different mean standard deviations ΔE. (Note that any $E_0 c_n$ term on the r.h.s. of Eq. (12) with constant E_0 can be eliminated by a gauge transformation $c_n \rightarrow \exp(-iE_0 t/\tau)c_n$.)

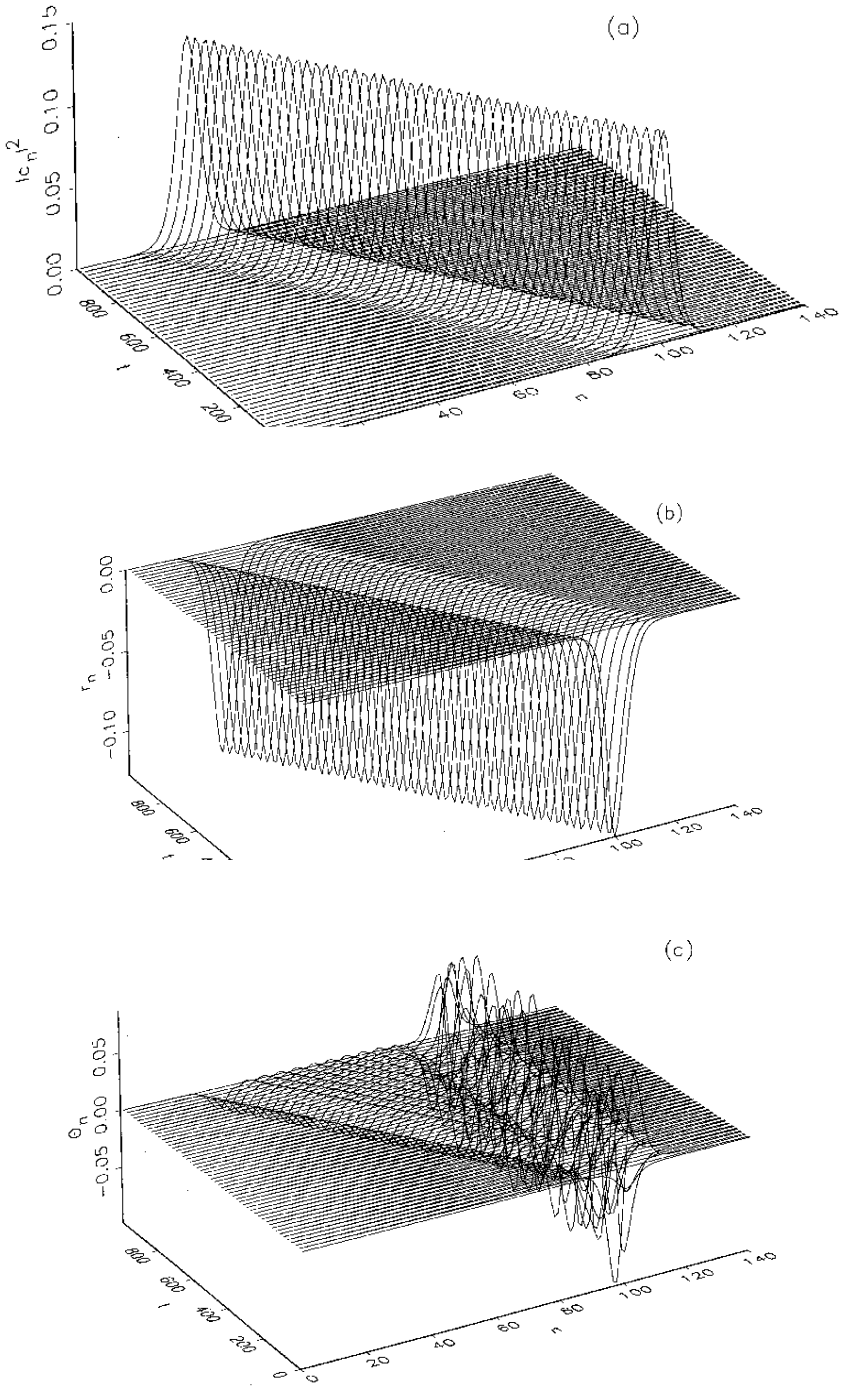

Fig. 3. Breather motion along the DNA in the ordered case. Motion is initiated by an initial kick of the velocities $\{\dot{r}_n\}$ directed along the corresponding pinning mode component. The kick amplitude is $\lambda_r = 0.25$.
(a) Uniformly moving electronic breather.
(b) The associated moving breather in the radial displacements.
(c) The angular breather contribution consisting of a small amplitude breather pinned at the starting site and a relatively large amplitude moving breather component propagating in alliance with the electron and radial breathers.

Generally the localized excitation patterns do not change qualitatively when diagonal disorder is taken into account. Compared with the ordered case one merely observes a shift of the excitation peak away from the central lattice site depending on the respective realization of the random potential. However, since in the presence of diagonal disorder the translational invariance of the lattice system is broken the localized amplitude pattern is no longer reflection symmetric with respect to a distinguished lattice site as opposed to the corresponding symmetric localized state of the ordered system. Moreover we find that the combined effect of the two localization mechanisms, viz. nonlinear polaron and linear Anderson-mode formation respectively, leads to enhancement of the degree of localization compared to the case when only one of the two mechanisms acts.

Furthermore, real DNA molecules exhibit random structural imperfections of their double helix caused e.g. by the random base sequence, the deforming impact of the chemical surroundings when DNA gets buffeted by water molecules and/or the varying hydrophobic potential of the base pair interactions depending on the ambient aqueous solvent that may leave the involved helix structures in irregularly distorted shapes. Accordingly, the structural disorder is incorporated in our model by randomly distributed equilibrium positions of the bases so that the resulting irregular helical DNA matrix deviates from the perfectly regular helix structure.

To be precise, we consider randomly distributed torsional coordinates $\theta_{n\,n-1}$ and radii r_n. Since the positions (actually, the distances) govern the value of the corresponding transfer matrix elements $V_{n\,n-1} = V_0\,(1 - \alpha d_{n\,n-1})$ nondiagonal disorder is induced in the latter at the same time. Random transfer integrals along the helix were used to represent random base pair sequences for which the charge transport along DNA was discussed recently in a model relying on localized electron states [15].

4 Charge transport mediated by mobile polarons and breathers

In this section we study the charge transport supported by mobile polarons respectively breathers propagating along DNA. To activate polaron motion an established method is provided by proper stimulation of localized internal normal modes of certain shape and frequency which are also called pinning modes [40]. The identification of possibly existing pinning modes is related to the linear stability analysis of the polarons. In order to investigate the stability of the polarons with respect to linear perturbations we derive the linearized system for which we impose small perturbations on the stationary polaron solution $(\Phi_n,\, r_n^{(0)}, \theta_n^{(0)})$ in the form:

$$c_n(t) = [\,\Phi_n + \delta c_n(t)\,]\,\exp(-i\,Et/\tau) \tag{21}$$
$$r_n(t) = r_n^{(0)} + \delta r_n(t) \tag{22}$$
$$\theta_n(t) = \theta_n^{(0)} + \delta\theta_n(t)\,, \tag{23}$$

where δc_n, δr_n and $\delta\theta_n$ are small time-dependent variables. Substitution of (21)-(23) into Eqs. (12)-(14) and retaining only the terms linear in the perturbations results in the system of tangent equations. The stability analysis is then performed using Floquet theory.

To this end we integrate the linear system of the tangent equations over one period $T = 2\pi\,\tau/E$ yielding the Floquet map

$$\delta x(nT) = F^n\,\delta x(0)\,, \tag{24}$$

with the Floquet matrix F determining the evolution of the initial set of variables $x(0) = (Re\delta c_n(0), Im\delta c_n(0), \delta r_n(0), \delta\dot{r}_n(0), \delta\theta_n(0), \delta\dot{\theta}_n(0))$ after times nT. To ensure linear stability all eigenvalues $\exp(i\,\psi_n)$ of the Floquet matrix F have to lie on the unit circle, i.e. the Floquet arguments ψ_n have to be real-valued. Intensive numerical investigations in a wide parameter range have proved that all the polarons gained from the map method are linearly stable.

Moreover the Floquet analysis supplies the frequencies of the normal modes via the relation $\omega_\psi = \omega[\psi/(2\pi) + m]$ with ψ expressed in *rad* and m is an arbitrary integer number. We identified the pinning modes for given sets of parameters. According to [40] we initiate the motion of polarons through suitable perturbations of the velocity variables $\dot{r}_n(t)$ and/or $\dot{\theta}_n$ targeted in the direction of the pinning mode, that is we use for the numerical integration of the system (12)-(14) the following initial conditions

$$\left\{\,\Phi_n, 0, r_n^{(0)}, 0, \theta_n^{(0)}, 0\,\right\} + \{0, 0, 0, \lambda_r\xi_r, 0, \lambda_\theta\xi_\theta\}\ , \tag{25}$$

with the normalized momentum parts $\xi_{r,\theta}$ of the pinning mode and $\lambda_{r,\theta}$ are the perturbation strengths (for details see [40]).

Ordered case

In Fig. 3 we present results for the activation of breather motion along DNA in the ordered case. We integrated the set of coupled nonlinear equations (12)-(14) with a fourth-order Runge-Kutta method and the accuracy of the computation was checked through monitoring the conservation of the total energy as well as the norm $\sum_n |c_n(t)|^2 = 1$. The applied kicking strength is $\lambda_r = 0.02$ corresponding to an amount of radial kinetic energy of the order of $200\,meV$. Interestingly, we found that there exists no angular pinning mode component ξ_θ (see further below) so that alone the excitation of the radial component ξ_r produces long-lived stable polaron and breather motions. Hence, our findings suggest that higher frequency radial fluctuational modes

of DNA instigate the propagation of localized structures along DNA rather than low frequency twist fluctuational modes. The Fig. 3 (a) demonstrates that the electronic component of the polaron moves with uniform velocity along the lattice maintaining its localized shape throughout the journey. In the same manner the radial polaron part travels as a localized wave along the strand so that the electron propagation is accompanied by a local and temporal contraction of the radii. However, the angular static polaron component splits up into two parts when the radial pinning mode is initially imposed. At the starting position there remains a standing breather of comparatively large amplitudes which reverse periodically their sign in the course of time. Thus the helix experiences alternately a local winding and unwinding around its central base pair. In addition a second breather of relatively small and exclusively negative amplitude propagates in unison with the electronic and radial polaron components. The result is that the region of the helix which is traversed by the electron gets locally untwisted. As the quantitative assessment of the charge transport is concerned we note that the breather travels across seventy sites (base pairs) in a thousand (dimensionless) time units meaning that physically the charge conduction across the base pairs of DNA over a distance of $238\mathring{A}$ takes $\sim 0.16ns$ leading to a higher transport rate than a typical one found for protein conductivity [15]. This underlines the status ascribed to DNA molecules as promising candidates establishing fast and efficient charge transport in (albeit only theorized yet) molecular electronical engineering utilizing them as molecular wires.

Static diagonal disorder

In the presence of diagonal static disorder, that is when the on-site electronic energies E_n^0 are represented by random numbers distributed in the interval $|E_n^0| < \Delta E$ with width ΔE, we find that mobile breathers exist up to a critical degree of disorder ΔE_{crit} and conductivity persists. (Let us stress that it was indeed experimentally found that the random sequence $\lambda-$DNA is an electrical conductor [9].) Beyond this critical value continuous propagation of the breathers along the lattice is prevented.

This behavior is illustrated in Fig. 4 displaying the spatio-temporal evolution of the electronic amplitude $|c_n(t)|^2$. While for a relatively small amount of disorder $\Delta E = 0.05$ the electronic breather (together with its radial and torsional counterparts) is able to travel uniformly along the lattice for a ten times increased $\Delta E = 0.5$ the breather motion is restricted to a neighborhood of the initially excited position around which it wanders in an oscillatory manner.

Regarding mobility there act two competing mechanisms in the combined disordered nonlinear system, namely a linear Anderson-type one related with the effects of disorder which attempts to pin the modes (bear in mind that the linear Anderson-modes are supposed to be immobile) and opposed to this

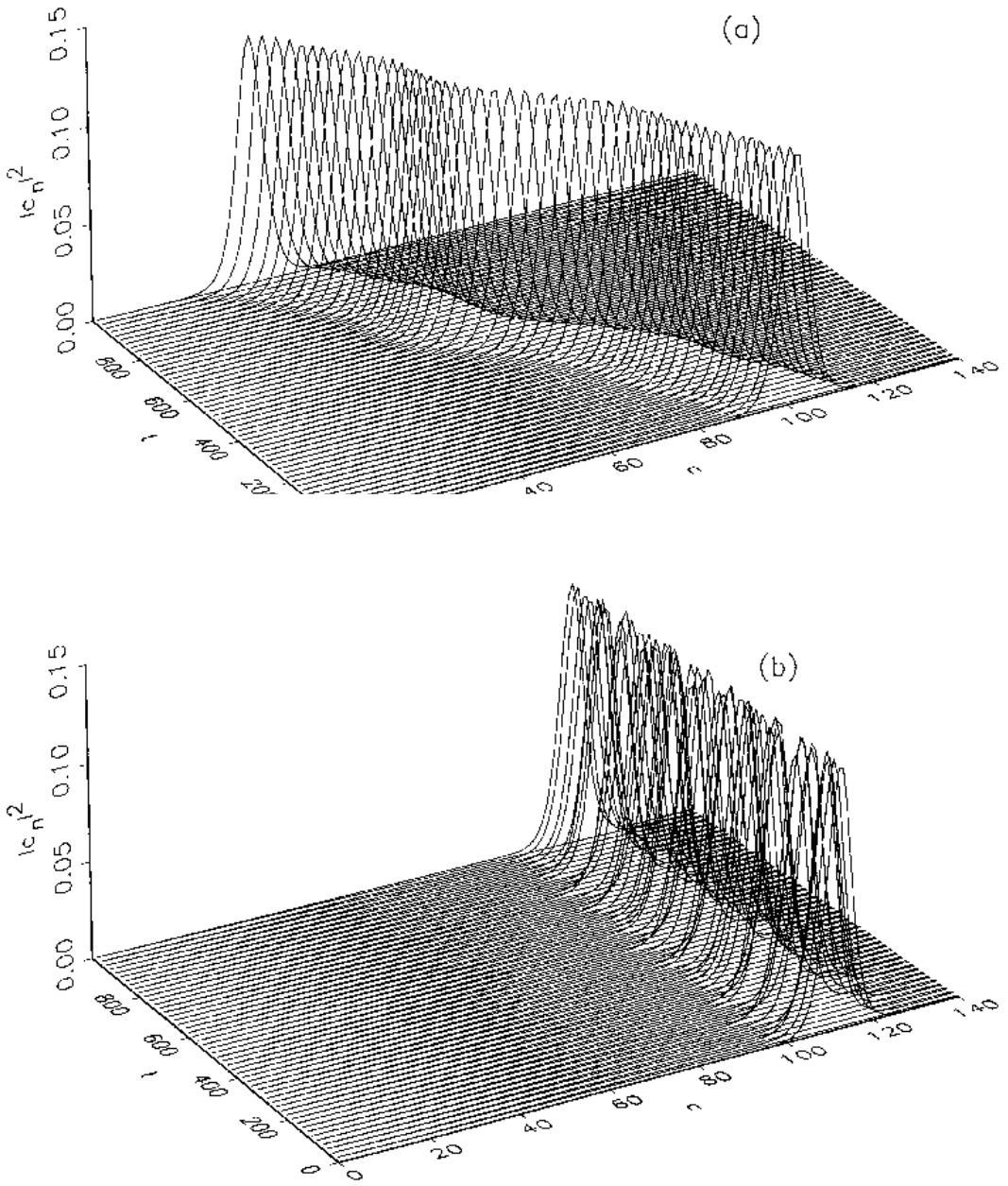

Fig. 4. Electron breather motion along DNA with diagonal disorder for two different values of the width ΔE of the random distribution of the on-site electronic energy $|E_n^0|$.
(a) Width $\Delta E = 0.05$. The electron breather moves with uniform velocity along a strand.
(b) Width $\Delta E = 0.5$. Confined electron breather with positions oscillating itinerantly around the initial lattice position.

there operates the nonlinear mechanism utilizing the pinning mode to activate motion. The relative strength of these two mechanisms $\Delta E/\lambda_r$ determines then breather mobility. In order to summarize the results for the breather mobility in the presence of diagonal disorder we display in 5 the temporal behavior of

the first momentum of the electronic occupation probability defined as

$$\bar{n}(t) = \sum n|c_n(t)|^2 \,, \tag{26}$$

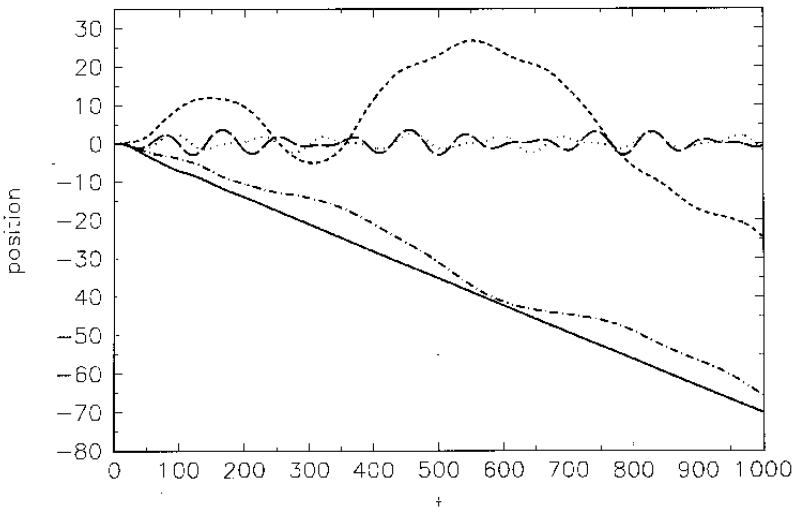

Fig. 5. Diagonal disorder. The position of the center of the electron breather as a function of time and for different amounts of disorder. Full line (Ordered case), short dashed line ($\Delta E = 0.025$), dashed-dotted line ($\Delta E = 0.050$), dotted line ($\Delta E = 0.100$) and long dashed line ($\Delta E = 0.500$).

which determines the position of the breather center as a function of time. The breathers are mobile and propagate unidirectionally with (virtually) constant velocity along the lattice up to an amount of disorder $\Delta E \simeq 0.045$. Generally, the larger the width ΔE the lower becomes this velocity. Finally, for an overcritical amount of disorder the breather performs oscillatory motions around its starting lattice position. The frequency of these oscillations diminishes gradually with more enlarged ΔE and simultaneously the excursions from the starting site get continuously stronger confined. Despite the non-directed character of its motion even for a moderate amount of disorder $\Delta E = 0.05$ the breather is able to travel as far as twenty lattice sites away from its starting position. Eventually linear Anderson-type disorder effects overwhelm more and more the nonlinear activation mechanism for breather motion through the excitation of the nonlinear pinning mode.

Random double helix structure

Concerning the impact of structural disorder we considered random distributions of the base pair spacings $r_n - r_0 \in [-\Delta, \Delta]$ and the twist angles $\theta_n - \theta_0 \in [-\Delta, \Delta]$ with different mean standard deviations Δ.

For representative results we averaged over several realizations of structural disorder. The results for the temporal evolution of the electron breather center

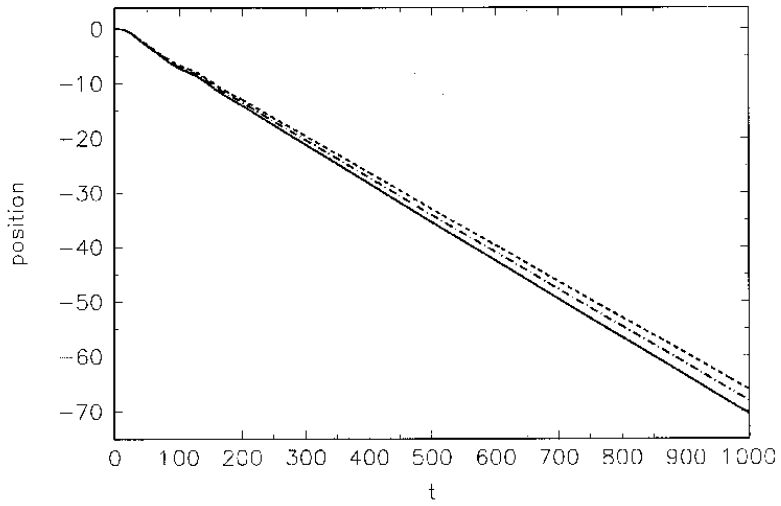

Fig. 6. Structural disorder and random double helix structure. The temporal behavior of the position of the electron breather center for different degrees of randomness in the radii r_n and angles θ_n. Assignment of the line types to the increasing mean standard deviations ranging up to 10% of the respective mean value: Full line (1%), dashed dotted line (5%) and dashed line (10%).

are depicted in Fig. 6. We conclude that structural disorder does not significantly affect the mobility of the breathers. For growing degree of disorder merely the propagation velocity gets reduced. Even in the case of fairly strong disorder $\Delta = 10\%$ (dashed line) the breather is still able to propagate steadily.

We studied also the polaron mobility under the impact of combined static diagonal and structural disorder and found that the strong pinning effect generated by static diagonal disorder prevails over the more harmless and merely velocity-reducing influence of structural irregularities. Particularly the last result is in compliance with the findings in [41] where it was reported that hopping conductivity in proteins and DNA is influenced first of all by the molecular conformations and not by their sequences.

5 Floquet analysis

It is instructive to consider also the linear limit case of the coupled nonlinear electron-vibration system even though the results obtained throughout this paper bear essentially nonlinear character. The study of the linear limit system itself and its Floquet analysis can be applied as a reference and as a tool for obtaining useful information for the interpretation of the Floquet analysis of the fully nonlinear system.

5.1 The linear system

The linear limit system is derived from the Eqns. (12)-(14) for $\alpha = k = 0$ giving

$$i\,\tau\,\dot{c}_n = -c_{n+1} - c_{n-1} \tag{27}$$
$$\ddot{r}_n = -r_n \tag{28}$$
$$\ddot{\theta}_{n\,n-1} = -\Omega^2\,\theta_{n\,n-1} \tag{29}$$

In the first equation the terms $E_n^0\,c_n$, which in a homogeneous system reduce to $E_0\,c_n$, have been eliminated through the gauge transformation $c_n \rightarrow c_n \exp(-i\,E_0\,t/\tau)$. In the linear limit the electronic and vibrational degrees of freedom are decoupled.

To construct the electronic state we substitute in Eq. (27), $c_n(t) = \phi_n \exp(-iE\,t/\tau)$ with time-independent ϕ_n yielding the linear stationary discrete Schrödinger equation: $E\,\phi_n = -\phi_{n+1} - \phi_{n-1}$. With the Bloch mode solutions $\phi_n = \exp(i\,q\,n)$ we get then the dispersion relation: $E = -e^{i\,q} - e^{-i\,q} = -2\,\cos q$. The linear electronic energy spectrum runs from -2 to 2. The polaron in the full system displayed in Fig. 2 possesses an energy value $E = -2.064$ which is slightly below the lower band edge $E = -2$ assigned to a wave number $q = 0$ and in the linear regime the frequencies are in the range $w_p = E/\tau \in [-7.75, 7.75]$. Conclusively, the time scale for the evolution of the angular (radial) variables $\theta_{n\,n-1}$ (r_n) represented by independent harmonic oscillators with frequencies 1 and $\Omega = 0.0842$, respectively, is two orders (one order) of magnitude larger than the one of the electron.

The linear analysis is also useful to understand the origin of many of the numerically calculated Floquet arguments for the fully nonlinear system. The values of the variables r_n and $\theta_{n\,n-1}$ after a period $T = 2\,\pi/w_p = 2\,\pi\,\tau/E$ are: $r_n(T) = \exp(i\,2\,\pi\,/w_p)\,r_n(0)$ and $\theta_{n\,n-1}(T) = \exp(i\,2\,\pi\,\Omega/w_p)\,\theta_{n\,n-1}(0)$. Therefore, their corresponding Floquet arguments are given by $2\,\pi/w_p$ and $2\,\pi\,\Omega/w_p$, for r_n and $\theta_{n\,n-1}$, respectively, which are attributed to angular positions in the complex plane with values around $\pm 45^0$ and $\pm 3.9^0$ for polarons with energies slightly below $E = -2$ and with increased $|E|$ these angular positions shift to lower values on the unit circle.

5.2 Results of the Floquet analysis

The numerical integration of the system of tangent equations over one period of the polaron's oscillation $T = 2\,\pi\,\tau/|E|$ allows us to obtain the actual Floquet matrix. Its eigenvalues can be written as $\exp(i\,\psi_n)$ with ψ_n being the Floquet

arguments. The system is linearly stable provided all the Floquet arguments are real. As noted earlier in this paper within the range of parameters studied in this paper linear stability is assured, but this is not the only information that can be gained from the Floquet analysis.

In order to relate the positions of the numerous eigenvalues of the Floquet matrix in the complex plane to the various degrees of freedom contained in the system it is elucidating to study first an anti-coupling limit in the electronic subsystem. Introducing an auxiliary tunable coupling parameter $0 \leq \mu \leq 1$, which corresponds to the transfer integral in the scaled system, the anti-coupling limit is obtained with $\mu = 0$ and the actually studied coupled system with $\mu = 1$.

For the decoupled electron system ($\mu = 0$) the value of the energy E can be easily derived with the help of the Eqs. (15) and (19), giving $E\Phi_n = -k^2|\Phi|^2\Phi_n$ and $r_n^{(0)} = -k|\Phi_n|^2$, which leads to $E = -1$ for the localized state $\Phi_n = \delta_{n\,0}$ and $k = 1$ as a typical value. Therefore, the r_n-multipliers are in the vicinity of $\pi/2$, the $\theta_{n\,n-1}$'s lie at small angles at both sides of $(1, 0)$ and the c_n's are located at $(1, 0)$ on the unit circle, in accordance with the analysis performed in 5.1. As we switch on the coupling μ and increase it up to the actual value $\mu = 1$, we can follow the evolution of the multipliers. Eventually, for $\mu = 1$ the r_n's and $\theta_{n\,n-1}$'s have moved to positions with about half their initial angle values while spreading a little on the unit circle (the $\theta_{n\,n-1}$'s to lesser extent though). The c_n's separate from $(1, 0)$ and invade the whole circle, as a consequence of the nonlinear coupling between the electron amplitudes and the vibrations. The exceptions are the pair at $(1, 0)$, corresponding to the phase mode, and another isolated pair close to this point. The latter pair is associated with the spatially antisymmetric pinning mode, responsible for the mobility of the polaron. Note that the linear approximation described in 5.1 is an approximation for the radial and angular variables. The Floquet multipliers for the decoupled and full systems, respectively are shown in Fig. 7.

In order to illuminate further the role played by the vibrational modes with respect to the initiation of mobility of the polaron we cast the Floquet matrix F in the form of a supermatrix formed by submatrices:

$$F = \begin{pmatrix} F_{c\,c} & F_{c\,r} & F_{c\,\theta} \\ F_{r\,c} & F_{r\,r} & F_{r\,\theta} \\ F_{\theta\,c} & F_{\theta\,r} & F_{\theta\,\theta} \end{pmatrix}, \tag{30}$$

and the indices of the submatrices refer to the origin of their entries. From the arguments of the eigenvalues of the submatrices an/or combinations of them, it is possible to deduce additional information about the spectral features attributed to the various degrees of freedom contained in the coupled nonlinear

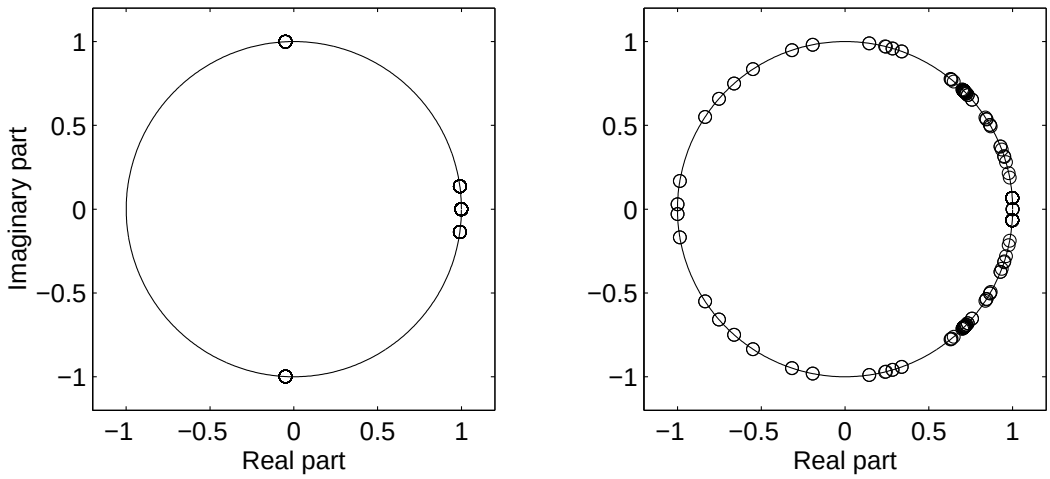

Fig. 7. The Floquet multipliers in the complex plane. Left figure: The linear limit system (27)-(29) at the anti-coupling limit $\mu = 0$. Right figure: The fully coupled nonlinear system.

system. The matrix F_{cc} appears in the Born-Oppenheimer approximation. To recover the pinning mode of the complete system it suffices to consider only the subsystem consisting of the electronic part coupled to the radial motions for which the Floquet matrix reduces to the submatrix $F_{CR} = (F_{cc}\ F_{cr}; F_{rc}\ F_{rr})$, which means that the mobility of the polaron is mainly a consequence of the coupling between the electron amplitudes and the radial variables and that the electron will not move within the Born-Oppenheimer approximation. The Figs. 8 and 9

illustrate these statements. The left (right) part of the Fig. 8 shows the multipliers of F_{rr} ($F_{\theta\theta}$). In comparison with the linear case studied in the preceding section we note that while the radial components of the multipliers shifted their positions to lower angles and exhibit some spread the angular multipliers hardly alter their position. Hence, perturbations of the angular twist motions in the context of the coupled system resemble the behavior of the linear limit system. The left part of Fig. 9 depicts the eigenvalues of F_{cr} in the vicinity of $(1, 0)$. The pair of pinning mode eigenvalues is recognizable. In the right part of the figure the normalized pinning mode is portrayed.

Moreover, it should be pointed out that for larger elongations of $\theta_{n\,n-1}$, beyond the range where the linear expansion of $d_{n\,n-1}$ is valid, there exists also an angular pinning mode as a consequence of the coupling between the electronic amplitudes and the angular variables.

The fact that the disorder eventually prevents the polaron from being moved can also be explained with the help of the Floquet multipliers. When the degree of disorder is increased the pinning mode eigenvalues move progressively away from $(1, 0)$ towards larger arguments ψ and approach the rest of the F_r

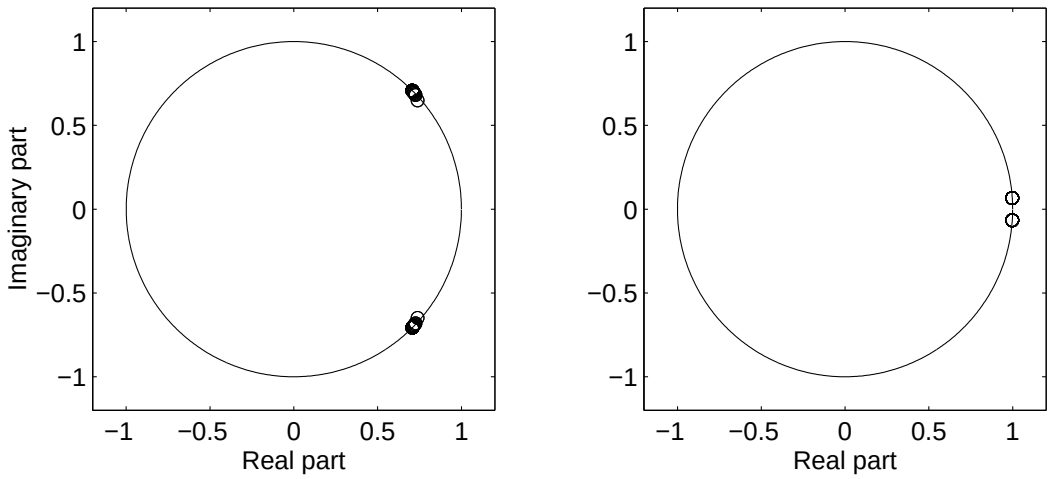

Fig. 8. Multipliers of F_{rr} (left figure) and $F_{\theta\theta}$ (right figure).

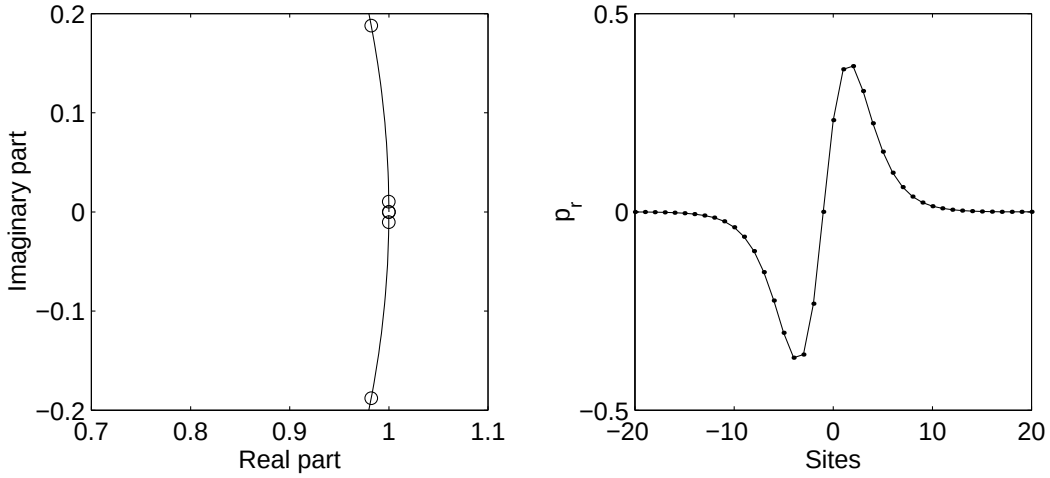

Fig. 9. Multipliers of F_{cr} in the vicinity of $(1, 0)$. The pinning mode eigenvalues are recognizable. The right part of the figure shows the normalized pinning mode.

eigenvalues. Fig. 10 displays the growth of the arguments of the pinning mode as a function of the disorder strength ΔE. Eventually the system is too far away from the instability due to the marginal mode, which appears when the pair of pinning mode eigenvalues collapses at $(1, 0)$. This is easy to understand, as the disorder brings about a decoupling of the variables, favoring localized, stationary, isolated modes.

6 Summary

In the present work we have studied an electron transfer mechanism in DNA relying on the coupling of the charge carrying unit to the vibrational modes of DNA responsible for the formation of polarons and electron-vibron breathers. The steric structure of the double helix of $\lambda-$DNA has been described in the context of the base-pair picture considering angular and radial vibrational

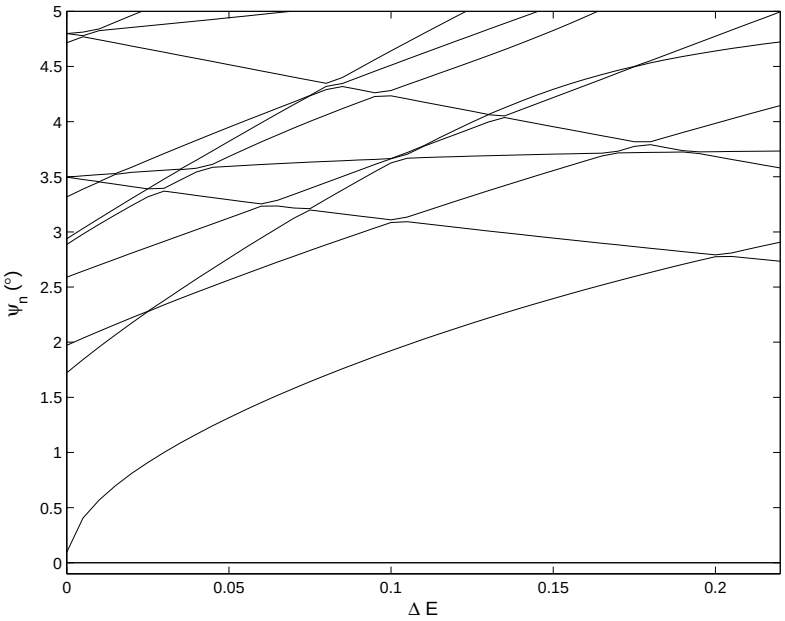

Fig. 10. Arguments of the Floquet multipliers of the low-frequency modes as a function of diagonal disorder ΔE demonstrating the growth of the argument of the pinning mode with increased amount of disorder so that the pinning mode eventually merges in the rest of the modes.

motions of the base pairs. We have focused interest on the initiation of long-range and stable polaron and breather motion along the DNA structure when static and/or structural disorder inherent to any real DNA molecule is taken into account. We remark that the proposed polaron-like transport mechanism applies to electron hole conduction too. In the first part of the paper we have constructed exact stationary localized solutions (polarons and static electron-vibron breathers) with the help of a nonlinear map approach. We have found that the interplay of disorder and nonlinearity amplifies the degree of localization in comparison with cases when either disorder or nonlinearity alone is present. With concern to mobile electron-vibron breather solutions, whose motion is activated through a kick mechanism utilizing the pinning mode, with the current work we have demonstrated that they are fairly robust when the electron-vibration system is subjected to randomness. Generally, even for a moderate amount of disorder the breathers retain their localized shapes and support directed, long-ranged coherent electron transfer along strands of the bent double helix. In particular the last result suggests that DNA seems suitable for the design of (one-dimensional) functional nanostructures as ingredients of molecular nanoelectronical devices. Furthermore, we have observed that the electron breather is accompanied by vibrational breathers in the radial as well as angular components, respectively causing local and temporal deformations of the traversed region of the double helix. Conclusively, efficient charge transport in DNA proceeds on the condition that the double helix undergoes structural changes which is exemplary for the interplay of structure

and function in flexible and adaptive biomolecules.

Acknowledgments

One of the authors (D.H.) acknowledges support by the Deutsche Forschungsgemeinschaft via a Heisenberg fellowship (He 3049/1-1). J.F.R.A. acknowledges D.H. and the Institut für Theoretische Physik for their warm hospitality. J.A. is grateful for a scholarship supplied by the Studienstiftung des deutschen Volkes. The authors are also grateful to the support under the LOCNET EU network HPRN-CT-1999-00163.

References

[1] D.D. Eley and D.I. Spivey, Trans. Faraday Soc. **58**, 411 (1962).

[2] C.A. Mirkin, R.L. Letsinger R.C. Mucic and J.J. Storhoff, Nature **382**, 607 (1996); A.A. Voityuk, N. Rösch, M. Bixon, and J. Jortner, J. Phys. Chem. **104**, 9740 (2000); F.C. Grozema, Y.A. Berlin and L.D.A. Siebbels, J. Am. Chem. Soc. **122** 10903 (2000); Y.A. Berlin, A.L. Burin and M.A. Ratner, J. Am. Chem. Soc. **123**, 260 (2001).

[3] M. Ratner, Nature **397**, 480 (1999).

[4] D.B. Hall, R.E. Holmkin and J.K. Barton, Nature **382**, 731 (1996).

[5] D.B. Hall and J.K. Barton, J. Am. Chem. Soc. **119**, 5045 (1997).

[6] M.R. Arkin, E.D.A. Stemp, S.C. Pulver and J.K. Barton, Chem. Biol. **4**, 369 (1997).

[7] Y. Okahata, T. Kobayashi, K. Tanaka, and M. Shimomura, J. Am. Chem. Soc. **120**, 6165 (1998).

[8] E. Meggers, M.E. Michel-Beyerle and B. Giese, J. Am. Chem. Soc. **120**, 12950 (1998).

[9] H.-W. Fink and C. Schönenberger, Nature **398**, 407 (1999).

[10] P. Tran, B. Alavi and G. Gruner, Phys. Rev. Lett. **85**, 1564 (2000).

[11] E. Braun, Y. Eichen, U. Sivan and G. Ben-Yoseph, Nature **391**, 775 (1998).

[12] D. Porath, A. Bezryadin, S. de Vries and C. Dekker, Nature **403**, 635 (2000).

[13] P.J. de Pablo, F. Moreno-Herrero, J. Colchero, J. Gómez Herrero, P. Herrero, A.M. Baró, P. Ordejón, J.M. Soler and E. Artacho, Phys. Rev. Lett. **85**, 4992 (2000).

[14] J. Jortner, M. Bixon, T. Langenbacher and M.E. Michel-Beyerle, Proc. Nat. Acad. Sci. USA **95**, 12759 (1998).

[15] Y.-J. Ye, R.-S. Chen, A. Martinez, P. Otto and J. Ladik, Sol. Stat. Comm. **112**, 139 (1999).

[16] R. Bruinsma, G. Grüner, M.R. D'Orsogna and J. Rudnick, Phys. Rev. Lett. **85**, 4393 (2000).

[17] Z.G. Yu and Xueyu Song, Phys. Rev. Lett. **86**, 6018 (2001).

[18] M. Hjort and S. Stafström, Phys. Rev. Lett. **87**, 228101-1 (2001).

[19] D. Ly et al, J. Am. Chem. Soc. **118**, 8747 (1996).

[20] J. Jortner, Proc. Nat. Acad. Sci. USA, **95**, 12759 (1998).

[21] E. Conwell and S.V. Rakhmanova, Proc. Nat. Acad. Sci. USA, **97**, 4556 (2000).

[22] D. Ly, L. Sanii and G.B. Schuster, J. Am. Chem. Soc., **121**, 9400 (1999).

[23] Z. Hermon, S. Caspi and E. Ben-Jacob, Europhys. Lett. **43**, 482 (1998).

[24] M. Peyrard and A.R. Bishop, Phys. Rev. Lett. **62**, 2755 (1989).

[25] L.V. Yakushevich, Quart. Rev. Biophys. **26**, 201 (1993).

[26] M. Barbi, S. Cocco and M. Peyrard, Phys. Lett. A **253**, 358 (1999).

[27] L. Stryer *Biochemistry*, (Freeman, New York, 1995).

[28] S. Cocco and R. Monasson, J. Chem. Phys. **112**, 10017 (2000).

[29] T.D. Holstein, Ann. Phys. NY **8**, 325, 343 (1959).

[30] P.W. Anderson, Phys. Rev. **109**, 1492 (1958).

[31] N.F. Mott, Adv. Phys. **10**, 107 (1961).

[32] D. Bambusi and A. Giorgilli, J. Stat. Phys. **71**, 569 (1993).

[33] D. Hennig, J. Math. Phys. **39**, 3568 (1998).

[34] R.S. MacKay and S. Aubry, Nonlinearity **7**, 1623 (1994).

[35] D. Hennig, in preparation.

[36] G. Kalosakas, S. Aubry and G.P. Tsironis, Phys. Rev. B **58**, 3094 (1998).

[37] N.K. Voulgarakis and G.P. Tsironis, Phys. Rev. B **63**, 14302 (2001).

[38] M. Peyrard and M.D. Kruskal, Physica D **14**, 88 (1984).

[39] S. Flach and C.R. Willis, Phys. Rep. **295**, 181 (1998).

[40] D. Chen, S. Aubry, and G.P. Tsironis, Phys. Rev. Lett. **77**, 4776 (1996).

[41] Y.-J. Ye and J. Ladik, Int. J. Quant. Chem. **52**, 491 (1994).